

Gravitational wave sources for Pulsar Timing Arrays

Ligong Bian,^{1,2,*} Shuailiang Ge,^{2,3,†} Jing Shu,^{3,2,4,‡} Bo Wang,⁵ Xing-Yu Yang,^{6,§} and Junchao Zong^{7,8}

¹*Department of Physics and Chongqing Key Laboratory for Strongly Coupled Physics, Chongqing University, Chongqing 401331, China*

²*Center for High Energy Physics, Peking University, Beijing 100871, China*

³*School of Physics and State Key Laboratory of Nuclear Physics and Technology, Peking University, Beijing 100871, China*

⁴*Beijing Laser Acceleration Innovation Center, Huairou, Beijing, 101400, China*

⁵*International Centre for Theoretical Physics Asia-Pacific,*

University of Chinese Academy of Sciences, 100190 Beijing, China

⁶*Quantum Universe Center (QUC), Korea Institute for Advanced Study, Seoul 02455, Republic of Korea*

⁷*Department of Physics, Nanjing University, Nanjing 210093, China*

⁸*CAS Key Laboratory of Theoretical Physics, Institute of Theoretical Physics, Chinese Academy of Sciences, Beijing 100190, China*

Very recently, several pulsar timing array collaborations, including CPTA, EPTA, and NANOGrav, reported their results from searches for an isotropic stochastic gravitational wave background (SGWB), with each finding positive evidence for SGWB. In this work, we assessed the credibility of interpreting the Hellings-Downs correlated free-spectrum process of EPTA, PPTA, and NANOGrav as either the result of supermassive black hole binary mergers or various stochastic SGWB sources that originated in the early Universe, including first-order phase transitions, cosmic strings, domain walls, and large-amplitude curvature perturbations. Our observations show that the current new datasets do not display a strong preference for any specific SGWB source based on Bayesian analysis.

I. INTRODUCTION

Pulsar timing array (PTA) experiments provide a unique window to probe the gravitational waves (GWs) at nano-Hertz frequencies, with possible sources being supermassive black hole binaries (SMBHBs) [1–5], curvature perturbations [6, 7], and new-physics models including first-order phase transition (FOPT) [8, 9], cosmic strings [10], and domain walls [11], etc.

Previously, hints of a stochastic common-spectrum process have been observed in the pulsar-timing datasets of NANOGrav [5], PPTA [12], EPTA [13] and IPTA [14], which has aroused enormous interests in the communities of astrophysics, cosmology, and particle physics. Since then, numerous interpretations have been proposed for such a stochastic common-spectrum process in the literature based on different models, including SMBHBs [15–17], cosmic strings [18–21], FOPT [22–25], domain walls [26, 27], and so on. Very recently, NANOGrav released their new 15-yr dataset [28–30], CPTA released their first data [31], EPTA release the second data [32], and PPTA released their third data set [33–35]. Therein, NANOGrav, EPTA, and CPTA inspiringly show positive evidence for the detection of stochastic gravitational-wave background (SGWB) in the common-spectrum process.

Compared to the previously observed common-spectrum process in the old NANOGrav 12.5-yr dataset and the results from other collaborations like EPTA and PPTA, this time we not only have robust evidence for the common-spectrum process, but also have positive evidence concerning the Hellings-Downs (HD) correlation, which provides direct evidence for the gravitational wave quadrupolar signal. In this Letter,

we incorporate the new PTA datasets from the three collaborations - PPTA, EPTA, and NANOGrav. We employ the Bayesian analysis method to contrast interpretations between different SGWB models and fit each model separately. Ultimately, we find no strong evidence favoring any potential cosmological sources (such as SMBHBs, etc) from the early Universe.

II. MODELS OF GENERATING SGWBs

We discuss five main mechanisms in the early Universe that can generate SGWB at nano-Hertz frequencies, which are 1) SMBHB, 2) FOPT, 3) cosmic strings, 4) domain walls, and 5) large amplitude curvature perturbations. We refer the readers to Ref. [26] and references therein for a summary of these models. For convenience, we have also summarized the GW spectra of the latter four models with corresponding references in the Appendix.

Centers of most galaxies likely host supermassive black holes, forming binary systems during galaxy mergers [36, 37]. These systems emit gravitational radiation, creating a Gravitational Wave Background (GWB) detectable in the PTA band. The GWB's properties depend on the SMBHBs' characteristics and evolution. For binaries purely evolving through GW emission, the power spectral density follows a power law with a spectral index of $-13/3$ [2], influenced by interactions with the local galactic environment [38].

FOPTs happening in the early Universe arise in many models beyond the Standard Model of particle physics. For example, they are usually associated with explaining the baryon asymmetry (see e.g., Ref. [39]). An FOPT can generate gravitational waves in multiple ways, including collisions of vacuum bubbles, relevant shocks in the plasma, sound waves in the plasma after bubble collisions, and the magnetohydrodynamic turbulence in the plasma after bubble collisions [40]. Here, following Ref. [26], we consider the scenario that

* lgbycl@cqu.edu.cn

† sge@pku.edu.cn

‡ jshu@pku.edu.cn

§ xingyuyang@kias.re.kr

sound-wave contribution dominates. The GW spectrum is mainly determined by the latent heat α_{PT} , the inverse time duration of FOPT β which is usually rescaled by the Hubble parameter H_n at the bubble nucleation temperature T_n (which is approximately T_* , the temperature when the GW are produced), and the velocity of expanding bubble wall in the plasma background v_b [40].

A cosmic string is a one-dimensional topological defect associated with a symmetry breaking, which is also predicted in many models beyond the Standard Model. Infinite strings will intersect and generate string loops [41]. The string loops can oscillate and vibrate to emit gravitational waves [42]. The strings can also develop the structure of kinks and cusps that can generate gravitational waves [43, 44]. GWs emitted from cosmic strings mainly depend on the parameters $G\mu$ and α_{CS} . G is the Newton gravitational constant and μ is the string tension (energy per unit length). α_{CS} is the loop-size parameter representing the ratio of the loop size to the Hubble length (or more naturally, the correlation length [45, 46]). Note we are discussing gauge strings associated with a gauge symmetry breaking, the energy of which is mainly lost in GWs, while the global strings associated with a global symmetry breaking lose energy mainly in the form of Goldstone bosons [47].

A domain wall is another kind of topological defects, which is two-dimensional. It is formed when discrete degenerate vacua are present after a symmetry breaking, which also naturally arises in many beyond-Standard-Model theories. The evolution of the domain wall network can generate gravitational waves; see e.g., Ref. [11]. To avoid the domain wall problem that domain walls dominate the Universe, a bias potential ΔV is usually introduced to kill the domain wall network by explicitly breaking the vacua degeneracy [48–50]. ΔV determines the time when the network disappears and thus marks the location of GW spectrum's peak frequency. Another key factor is the domain wall tension σ , i.e., the energy per unit wall area.

GWs can also be generated by the curvature perturbations due to the coupling at nonlinear order between scalar and tensor modes. Via the coupling with the tensor modes, scalar perturbations can induce GWs; see e.g., Refs. [6, 7, 51]. The power spectrum of curvature perturbations is assumed to be a power law, $P_{\mathcal{R}}(k) \propto P_{\mathcal{R}0}(k/k_*)^m$, where k is the wavenumber and k_* is the wavenumber at the frequency around 1yr^{-1} . The corresponding GW spectrum is then $\Omega_{\text{GW}}(k) \propto P_{\mathcal{R}}^2(k)$. The amplitude $P_{\mathcal{R}0}$ and the slope m are the two key parameters that determine the GW spectrum.

III. COMPARISONS AMONG SGWB MODELS

By using the fitting results of the free spectrum with the HD correlation from the datasets of NANOGrav, PPTA and EPTA, we can make comparisons between the following models: SMBHBs, FOPT, cosmic strings, domain walls, and scalar-induced GWs, which are labeled as M_i ($i = 1, 2, 3, 4, 5$) in sequence, respectively. We list the bayesian prior range of the model parameters in table. II and the results are summarized in Eqs. (1)-(3). In addition, the corresponding interpretation

of Bayes factors is shown in Table I.

EPTA and NANOGrav have a weak evidence while PPTA has a positive evidence in favor of the cosmic strings and FOPT explanations against SMBHBs. A positive evidence in favor of the SMBHB, cosmic strings, scalar-induced GWs, FOPT against domain walls is shown in all the datasets of EPTA, PPTA and NANOGrav. Especially, NANOGrav and PPTA show more inclination in favor of the FOPT explanation than the other sources, while EPTA are more sensitive to cosmic-string explanation.

Upon comparing these explanations, we find that none of the above models has a distinct advantage over others in interpreting the common-spectrum process with the HD correlation implied in the datasets of NANOGrav, PPTA and EPTA.

Table I. Bayes factors can be interpreted as follows: for comparing a candidate model M_i against another model M_j , a Bayes factor of 20 corresponds to a belief of 95% in the statement “ M_i is true”, which means a strong evidence in favor of M_i [52].

B_{ij}	Evidence in favor of M_i against M_j
1 – 3	Weak
3 – 20	Positive
20 – 150	Strong
≥ 150	Very strong

$$B_{ij}^{\text{NG15}} = \begin{pmatrix} 1 & 0.49 & 0.55 & 5.19 & 1.34 \\ 2.03 & 1 & 1.12 & 10.55 & 2.72 \\ 1.82 & 0.90 & 1 & 9.46 & 2.44 \\ 0.19 & 0.09 & 0.11 & 1 & 0.26 \\ 0.75 & 0.37 & 0.41 & 3.88 & 1 \end{pmatrix} \quad (1)$$

$$B_{ij}^{\text{PPTA}} = \begin{pmatrix} 1 & 0.27 & 0.32 & 2.53 & 0.58 \\ 3.64 & 1 & 1.16 & 9.2 & 2.10 \\ 3.13 & 0.86 & 1 & 7.92 & 1.81 \\ 0.40 & 0.11 & 0.13 & 1 & 0.23 \\ 1.73 & 0.48 & 0.55 & 4.37 & 1 \end{pmatrix} \quad (2)$$

$$B_{ij}^{\text{EPTA}} = \begin{pmatrix} 1 & 0.67 & 0.47 & 6.87 & 1.65 \\ 1.50 & 1 & 0.70 & 10.30 & 2.47 \\ 2.15 & 1.43 & 1 & 14.75 & 3.53 \\ 0.15 & 0.10 & 0.07 & 1 & 0.24 \\ 0.61 & 0.41 & 0.28 & 4.18 & 1 \end{pmatrix} \quad (3)$$

IV. CONSTRAINTS ON SGWB MODELS

In Fig. 1, we show the constraints on the log-amplitude $\log_{10} A$ of the SMBHB power-law spectrum. Analyses of PPTA, EPTA, and NANOGrav datasets yield the results $\log_{10} A \sim [-15.04, -14.42]$, $[-14.74, -14.42]$, and $[-14.76, -14.50]$ at 68% confidence level (C.L.), respectively.

Fig. 2 shows the result for the FOPT case from the Bayesian model fitting. The data constraint based on the PPTA dataset favors a moderate latent heat $\alpha_{PT} \geq 0.548$ and a duration $\beta/H_* \sim [9, 59]$ at the phase transition temperature

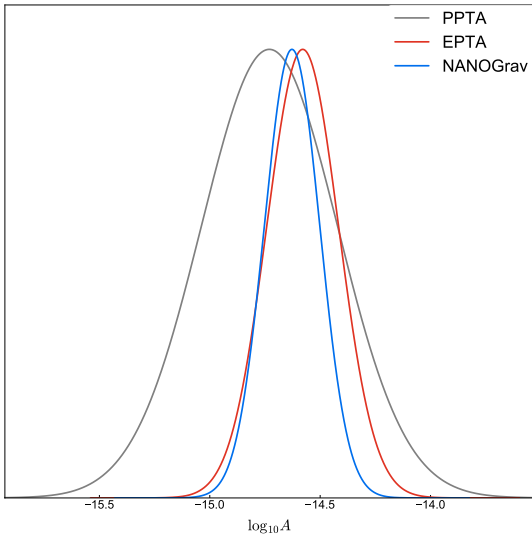


Figure 1. Constraints on the SMBHB parameter $\log_{10} A$ from the Bayesian model fitting.

$T_* \sim [0.61, 1.33]$ MeV at 68% C.L. Likewise, EPTA dataset at the same confidence level favors a latent heat $\alpha_{PT} \geq 0.591$, accompanied by a duration $\beta/H_* \sim [22, 40]$ at $T_* \sim [0.48, 1.30]$ MeV. Finally, the NANOGrav dataset at the same confidence level favors $\alpha_{PT} \geq 0.692$, $\beta/H_n \sim [29, 47]$, and $T_n \geq 1.03$ MeV. Noting that the energy injection from the phase transition would change the BBN and CMB observations [53, 54], which excludes some slow and strong phase transitions around $T_* \sim 1$ MeV.

The results based on the Bayesian model fitting for the case of cosmic string network are shown in Fig. 3. The constraints yield $\log_{10} G\mu \sim [-10.2, -7.5]$, $[-10.4, -8.0]$, and $[-10.9, -8.1]$ at 68% C.L. under PPTA, EPTA, and NANOGrav datasets, respectively, implying a $U(1)$ symmetry-breaking scale $\eta \sim \mathcal{O}(10^{13-14})$ GeV of local strings. Meanwhile, we also obtain constraints on the loop-size parameter α_{CS} that $\log_{10} \alpha_{CS} \sim [-5.5, -1.5]$, $[-5.3, -1.5]$, and $[-4.4, -0.7]$ at 68% C.L. from PPTA, EPTA, and NANOGrav datasets, respectively, which are well below the typical value of $\alpha_{CS} = 0.1$ suggested by simulations [55, 56].

In Fig. 4, we show the results for the domain-wall case based on the Bayesian model fitting. At 68% C.L., we get tight bounds on the bias ΔV and the surface energy density σ : $\log_{10}(\sigma/\text{TeV}^3) \sim [2.98, 5.12]$, $\log_{10}(\Delta V/\text{MeV}^4) \leq 4.94$ under the PPTA dataset, $\log_{10}(\sigma/\text{TeV}^3) \sim [2.89, 5.56]$, $\log_{10}(\Delta V/\text{MeV}^4) \leq 5.26$ under the EPTA dataset, and $\log_{10}(\sigma/\text{TeV}^3) \sim [5.11, 6.50]$, $\log_{10}(\Delta V/\text{MeV}^4) \sim [5.50, 7.95]$ under the NANOGrav dataset. Thus, considering a Z_2 domain wall network as an example, the results imply that the symmetry breaking scale should be $\eta \lesssim 10^4$ TeV for $\sigma = 2\sqrt{2}\lambda\eta^3/3$ assuming the interaction coupling as $\lambda \sim \mathcal{O}(10^{-2})$.

In the case of scalar-induced GWs, we find $\log_{10} P_{\mathcal{R}0} \sim [-3.17, -1.67]$ and $m \sim [-1.27, 0.53]$ are allowed by the PPTA dataset, $\log_{10} P_{\mathcal{R}0} \geq -2.32$ and $m \sim [-0.12, 0.68]$

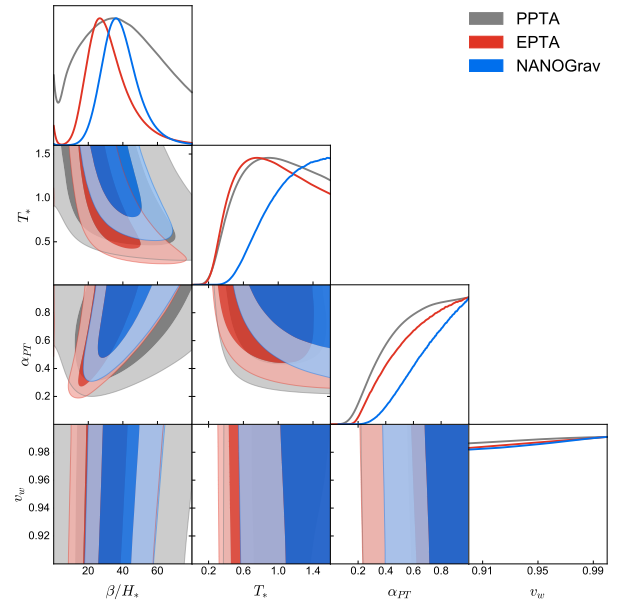


Figure 2. The constraints on parameters of FOPT from Bayesian model fitting. Contours contain 68% and 95% of the probability.

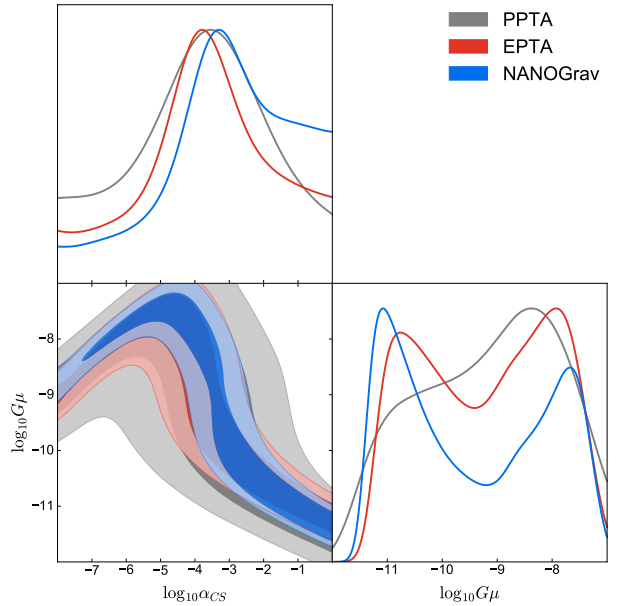


Figure 3. The constraints on parameters of cosmic strings from the Bayesian model fitting. Contours contain 68% and 95% of the probability.

are allowed by the EPTA dataset, $\log_{10} P_{\mathcal{R}0} \geq -2.03$ and $m \sim [0.19, 0.91]$ are allowed by the NANOGrav dataset at 68% C.L., as shown in Fig. 5. The slope m has a negative best-fit value from the PPTA dataset, which is consistent with the result from the old 12.5-yr NANOGrav dataset. However, positive best-fit values of m are obtained from the new datasets of EPTA and NANOGrav. None of these results shows a k^3 slope which was suggested as a universal infrared behavior

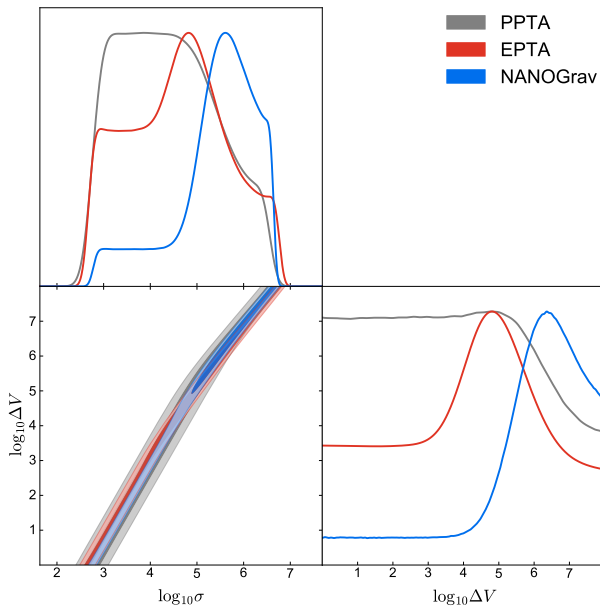


Figure 4. The constraints on parameters of domain wall from Bayesian model fitting. Contours contain 68% and 95% of the probability.

of GW spectrum [57]. The large amplitude curvature perturbations are also related to the formation of primordial black holes (PBHs), which are attractive dark matter candidates and are also the possible sources for the merger events of black hole binaries [58–60]. The best-fit value of amplitude $P_{\mathcal{R}0}$ from PPTA is similar to that from the old 12.5-yr NANOGrav dataset. In comparison, the new datasets of NANOGrav and EPTA give a larger best-fit value. The larger best-fit amplitude from new datasets implies a larger corresponding PBH abundance which can be even larger if the non-Gaussianity of curvature perturbations is considered [61–63].

V. CONCLUSION AND DISCUSSION

We consider different SGWB sources as the possible interpretations of the strong stochastic common-spectrum process with HD correlation observed by the NANOGrav, PPTA and EPTA collaborations. A Bayesian model comparison is carried out by fitting with the first 5 low-frequency bins of their HD free-spectrum data. Our results show that the current datasets from the three collaborations are all unable to distinguish one SGWB model as being obviously superior to the others. We also place constraints on the parameter spaces of SMBHBs, FOPT, cosmic strings, domain walls, and curvature fluctuations, some of which can be further used to constrain the related new physics. Our study mainly indicates that: 1) parameter spaces of the slow phase transition are with moderate strength around 1 MeV scale, which can be further constrained by BBN and CMB observations; 2) cosmic strings are formed after the $U(1)$ symmetry breaking scale around $\eta \sim \mathcal{O}(10^{13-14})$ GeV; 3) the discrete symmetry break-

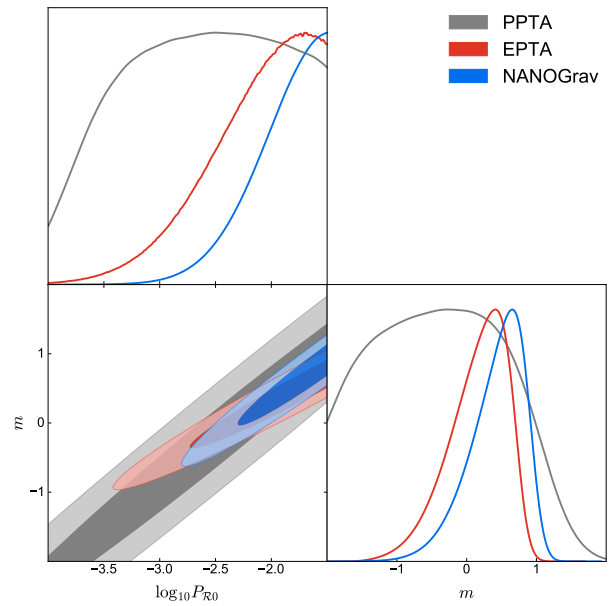


Figure 5. The constraints on parameters of power spectrum of curvature perturbations from the Bayesian model fitting. Contours contain 68% and 95% of the probability.

ing scale should be lower than 10^4 TeV; 4) the PBHs from curvature perturbations are severely constrained. In addition, we find that compared to EPTA and PPTA, the current data from NANOGrav can place much stronger constraints on SGWB model parameters.

Since all the cosmological SGWB models can reproduce the HD signal observed in the current datasets, more data from pulsar timing array are necessary to distinguish these models from SMBHBs. We further note that, more accurate GW spectrum based on numerical simulations and more accurate theoretical prediction of GW model parameters based on particle physics (such as the symmetry breaking scale for phase transitions, cosmic string, and domain wall) are also definitely crucial to settle down conclusively the preferred SGWB model(s).

ACKNOWLEDGMENTS

This work is supported by the National Key Research and Development Program of China under Grant No. 2020YFC2201501 and 2021YFC2203004. L.B. is supported by the National Natural Science Foundation of China (NSFC) under Grants No. 12075041 and No. 12147102, the Fundamental Research Funds for the Central Universities of China under Grants No. 2021CDJQY-011 and No. 2020CDJQY-Z003. S.G. is supported by NSFC under Grant No. 12247147, the International Postdoctoral Exchange Fellowship Program, and the Boya Postdoctoral Fellowship of Peking University. J.S. is supported by Peking University under startup Grant No. 7101302974 and the National Natural Science Foundation of China under Grants No. 12025507, No.12150015; and is sup-

ported by the Key Research Program of Frontier Science of the Chinese Academy of Sciences (CAS) under Grants No.

ZDBS-LY-7003 and CAS project for Young Scientists in Basic Research YSBR-006. XYY is supported in part by the KIAS Individual Grant QP090701.

-
- [1] M. Rajagopal and R. W. Romani, *Astrophys. J.* **446**, 543 (1995), [arXiv:astro-ph/9412038](#).
- [2] E. S. Phinney, (2001), [arXiv:astro-ph/0108028](#).
- [3] A. H. Jaffe and D. C. Backer, *Astrophys. J.* **583**, 616 (2003), [arXiv:astro-ph/0210148](#).
- [4] J. S. B. Wyithe and A. Loeb, *Astrophys. J.* **590**, 691 (2003), [arXiv:astro-ph/0211556](#).
- [5] Z. Arzoumanian *et al.* (NANOGrav), *Astrophys. J. Lett.* **905**, L34 (2020), [arXiv:2009.04496 \[astro-ph.HE\]](#).
- [6] K. N. Ananda, C. Clarkson, and D. Wands, *Phys. Rev. D* **75**, 123518 (2007), [arXiv:gr-qc/0612013](#).
- [7] D. Baumann, P. J. Steinhardt, K. Takahashi, and K. Ichiki, *Phys. Rev. D* **76**, 084019 (2007), [arXiv:hep-th/0703290](#).
- [8] A. Kosowsky, M. S. Turner, and R. Watkins, *Phys. Rev. Lett.* **69**, 2026 (1992).
- [9] C. Caprini, R. Durrer, and X. Siemens, *Phys. Rev. D* **82**, 063511 (2010), [arXiv:1007.1218 \[astro-ph.CO\]](#).
- [10] X. Siemens, V. Mandic, and J. Creighton, *Phys. Rev. Lett.* **98**, 111101 (2007), [arXiv:astro-ph/0610920](#).
- [11] T. Hiramatsu, M. Kawasaki, and K. Saikawa, *JCAP* **02**, 031 (2014), [arXiv:1309.5001 \[astro-ph.CO\]](#).
- [12] B. Goncharov *et al.*, *Astrophys. J. Lett.* **917**, L19 (2021), [arXiv:2107.12112 \[astro-ph.HE\]](#).
- [13] S. Chen *et al.*, *Mon. Not. Roy. Astron. Soc.* **508**, 4970 (2021), [arXiv:2110.13184 \[astro-ph.HE\]](#).
- [14] J. Antoniadis *et al.*, *Mon. Not. Roy. Astron. Soc.* **510**, 4873 (2022), [arXiv:2201.03980 \[astro-ph.HE\]](#).
- [15] V. Vaskonen and H. Veermäe, *Phys. Rev. Lett.* **126**, 051303 (2021), [arXiv:2009.07832 \[astro-ph.CO\]](#).
- [16] V. De Luca, G. Franciolini, and A. Riotto, *Phys. Rev. Lett.* **126**, 041303 (2021), [arXiv:2009.08268 \[astro-ph.CO\]](#).
- [17] K. Kohri and T. Terada, *Phys. Lett. B* **813**, 136040 (2021), [arXiv:2009.11853 \[astro-ph.CO\]](#).
- [18] J. Ellis and M. Lewicki, *Phys. Rev. Lett.* **126**, 041304 (2021), [arXiv:2009.06555 \[astro-ph.CO\]](#).
- [19] S. Blasi, V. Brdar, and K. Schmitz, *Phys. Rev. Lett.* **126**, 041305 (2021), [arXiv:2009.06607 \[astro-ph.CO\]](#).
- [20] R. Samanta and S. Datta, *JHEP* **05**, 211 (2021), [arXiv:2009.13452 \[hep-ph\]](#).
- [21] L. Bian, J. Shu, B. Wang, Q. Yuan, and J. Zong, *Phys. Rev. D* **106**, L101301 (2022), [arXiv:2205.07293 \[hep-ph\]](#).
- [22] Y. Nakai, M. Suzuki, F. Takahashi, and M. Yamada, *Phys. Lett. B* **816**, 136238 (2021), [arXiv:2009.09754 \[astro-ph.CO\]](#).
- [23] A. Addazi, Y.-F. Cai, Q. Gan, A. Marciano, and K. Zeng, *Sci. China Phys. Mech. Astron.* **64**, 290411 (2021), [arXiv:2009.10327 \[hep-ph\]](#).
- [24] W. Ratzinger and P. Schwaller, *SciPost Phys.* **10**, 047 (2021), [arXiv:2009.11875 \[astro-ph.CO\]](#).
- [25] X. Xue *et al.*, *Phys. Rev. Lett.* **127**, 251303 (2021), [arXiv:2110.03096 \[astro-ph.CO\]](#).
- [26] L. Bian, R.-G. Cai, J. Liu, X.-Y. Yang, and R. Zhou, *Phys. Rev. D* **103**, L081301 (2021), [arXiv:2009.13893 \[astro-ph.CO\]](#).
- [27] R. Z. Ferreira, A. Notari, O. Pujolas, and F. Rompineve, *JCAP* **02**, 001 (2023), [arXiv:2204.04228 \[astro-ph.CO\]](#).
- [28] G. Agazie *et al.* (NANOGrav), (2023), [10.3847/2041-8213/acdac6](#), [arXiv:2306.16213 \[astro-ph.HE\]](#).
- [29] A. Afzal *et al.* (NANOGrav), *Astrophys. J. Lett.* **951** (2023), [10.3847/2041-8213/acdc91](#), [arXiv:2306.16219 \[astro-ph.HE\]](#).
- [30] G. Agazie *et al.* (NANOGrav), *Astrophys. J. Lett.* **951** (2023), [10.3847/2041-8213/acda9a](#), [arXiv:2306.16217 \[astro-ph.HE\]](#).
- [31] H. Xu *et al.*, (2023), [10.1088/1674-4527/acdfa5](#), [arXiv:2306.16216 \[astro-ph.HE\]](#).
- [32] J. Antoniadis *et al.*, (2023), [arXiv:2306.16214 \[astro-ph.HE\]](#).
- [33] D. J. Reardon *et al.*, (2023), [10.3847/2041-8213/acdd02](#), [arXiv:2306.16215 \[astro-ph.HE\]](#).
- [34] D. J. Reardon *et al.*, (2023), [10.3847/2041-8213/acdd03](#), [arXiv:2306.16229 \[astro-ph.HE\]](#).
- [35] A. Zic *et al.*, (2023), [arXiv:2306.16230 \[astro-ph.HE\]](#).
- [36] J. Kormendy and L. C. Ho, *Ann. Rev. Astron. Astrophys.* **51**, 511 (2013), [arXiv:1304.7762 \[astro-ph.CO\]](#).
- [37] K. Akiyama *et al.* (Event Horizon Telescope), *Astrophys. J. Lett.* **875**, L1 (2019), [arXiv:1906.11238 \[astro-ph.GA\]](#).
- [38] M. C. Begelman, R. D. Blandford, and M. J. Rees, *Nature* **287**, 307 (1980).
- [39] D. E. Morrissey and M. J. Ramsey-Musolf, *New J. Phys.* **14**, 125003 (2012), [arXiv:1206.2942 \[hep-ph\]](#).
- [40] C. Caprini *et al.*, *JCAP* **04**, 001 (2016), [arXiv:1512.06239 \[astro-ph.CO\]](#).
- [41] T. Vachaspati and A. Vilenkin, *Phys. Rev. D* **30**, 2036 (1984).
- [42] T. Vachaspati and A. Vilenkin, *Phys. Rev. D* **31**, 3052 (1985).
- [43] T. Damour and A. Vilenkin, *Phys. Rev. Lett.* **85**, 3761 (2000), [arXiv:gr-qc/0004075](#).
- [44] T. Damour and A. Vilenkin, *Phys. Rev. D* **64**, 064008 (2001), [arXiv:gr-qc/0104026](#).
- [45] L. Sousa and P. P. Avelino, *Phys. Rev. D* **88**, 023516 (2013), [arXiv:1304.2445 \[astro-ph.CO\]](#).
- [46] Y. Gouttenoire, G. Servant, and P. Simakachorn, *JCAP* **07**, 032 (2020), [arXiv:1912.02569 \[hep-ph\]](#).
- [47] A. Vilenkin and T. Vachaspati, *Phys. Rev. D* **35**, 1138 (1987).
- [48] P. Sikivie, *Physical Review Letters* **48**, 1156 (1982).
- [49] G. B. Gelmini, M. Gleiser, and E. W. Kolb, *Physical Review D* **39**, 1558 (1989).
- [50] S. E. Larsson, S. Sarkar, and P. L. White, *Physical Review D* **55**, 5129 (1997).
- [51] K. Kohri and T. Terada, *Phys. Rev. D* **97**, 123532 (2018), [arXiv:1804.08577 \[gr-qc\]](#).
- [52] R. E. Kass and A. E. Raftery, *Journal of the American Statistical Association* **90**, 773 (1995).
- [53] Y. Bai and M. Korwar, *Phys. Rev. D* **105**, 095015 (2022), [arXiv:2109.14765 \[hep-ph\]](#).
- [54] S. Deng and L. Bian, (2023), [arXiv:2304.06576 \[hep-ph\]](#).
- [55] J. J. Blanco-Pillado, K. D. Olum, and B. Shlaer, *Phys. Rev. D* **89**, 023512 (2014), [arXiv:1309.6637 \[astro-ph.CO\]](#).
- [56] J. J. Blanco-Pillado and K. D. Olum, *Phys. Rev. D* **96**, 104046 (2017), [arXiv:1709.02693 \[astro-ph.CO\]](#).
- [57] R.-G. Cai, S. Pi, and M. Sasaki, *Phys. Rev. D* **102**, 083528 (2020), [arXiv:1909.13728 \[astro-ph.CO\]](#).
- [58] M. Sasaki, T. Suyama, T. Tanaka, and S. Yokoyama, *Phys. Rev. Lett.* **117**, 061101 (2016), [Erratum: *Phys. Rev. Lett.* **121**, 059901 (2018)], [arXiv:1603.08338 \[astro-ph.CO\]](#).
- [59] M. Sasaki, T. Suyama, T. Tanaka, and S. Yokoyama, *Class. Quant. Grav.* **35**, 063001 (2018), [arXiv:1801.05235 \[astro-](#)

- ph.CO].
- [60] B. Carr, K. Kohri, Y. Sendouda, and J. Yokoyama, *Rept. Prog. Phys.* **84**, 116902 (2021), arXiv:2002.12778 [astro-ph.CO].
 - [61] R.-g. Cai, S. Pi, and M. Sasaki, *Phys. Rev. Lett.* **122**, 201101 (2019), arXiv:1810.11000 [astro-ph.CO].
 - [62] N. Bartolo, V. De Luca, G. Franciolini, M. Peloso, D. Racco, and A. Riotto, *Phys. Rev. D* **99**, 103521 (2019), arXiv:1810.12224 [astro-ph.CO].
 - [63] R.-G. Cai, S. Pi, S.-J. Wang, and X.-Y. Yang, *JCAP* **10**, 059 (2019), arXiv:1907.06372 [astro-ph.CO].
 - [64] M. Hindmarsh, S. J. Huber, K. Rummukainen, and D. J. Weir, *Phys. Rev. Lett.* **112**, 041301 (2014), arXiv:1304.2433 [hep-ph].
 - [65] M. Hindmarsh, S. J. Huber, K. Rummukainen, and D. J. Weir, *Phys. Rev. D* **92**, 123009 (2015), arXiv:1504.03291 [astro-ph.CO].
 - [66] M. Hindmarsh, S. J. Huber, K. Rummukainen, and D. J. Weir, *Phys. Rev. D* **96**, 103520 (2017), [Erratum: Phys.Rev.D 101, 089902 (2020)], arXiv:1704.05871 [astro-ph.CO].
 - [67] J. Ellis, M. Lewicki, J. M. No, and V. Vaskonen, *JCAP* **06**, 024 (2019), arXiv:1903.09642 [hep-ph].
 - [68] J. Ellis, M. Lewicki, and J. M. No, *JCAP* **07**, 050 (2020), arXiv:2003.07360 [hep-ph].
 - [69] C. Caprini *et al.*, *JCAP* **03**, 024 (2020), arXiv:1910.13125 [astro-ph.CO].
 - [70] J. Ellis, M. Lewicki, and J. M. No, *JCAP* **04**, 003 (2019), arXiv:1809.08242 [hep-ph].
 - [71] H.-K. Guo, K. Sinha, D. Vagie, and G. White, *JCAP* **01**, 001 (2021), arXiv:2007.08537 [hep-ph].
 - [72] J. R. Espinosa, T. Konstandin, J. M. No, and G. Servant, *JCAP* **06**, 028 (2010), arXiv:1004.4187 [hep-ph].
 - [73] Y. Cui, M. Lewicki, D. E. Morrissey, and J. D. Wells, *JHEP* **01**, 081 (2019), arXiv:1808.08968 [hep-ph].
 - [74] Y. Gouttenoire, G. Servant, and P. Simakachorn, *JCAP* **07**, 016 (2020), arXiv:1912.03245 [hep-ph].
 - [75] S. Olmez, V. Mandic, and X. Siemens, *Phys. Rev. D* **81**, 104028 (2010), arXiv:1004.0890 [astro-ph.CO].
 - [76] K. Kadota, M. Kawasaki, and K. Saikawa, *JCAP* **10**, 041 (2015), arXiv:1503.06998 [hep-ph].
 - [77] R. Zhou, J. Yang, and L. Bian, *JHEP* **04**, 071 (2020), arXiv:2001.04741 [hep-ph].
 - [78] D. Foreman-Mackey, D. W. Hogg, D. Lang, and J. Goodman, *Publ. Astron. Soc. Pac.* **125**, 306 (2013), arXiv:1202.3665 [astro-ph.IM].
 - [79] A. Lewis, (2019), arXiv:1910.13970 [astro-ph.IM].

Appendix A: GW spectrum from different models

a. First-order phase transition (FOPT)

GW spectrum [40]:

$$\begin{aligned} \Omega_{\text{GW}}^{\text{sw}}(f)h^2 &= 2.65 \times 10^{-6} (H_* \tau_{\text{sw}}) \left(\frac{\beta}{H_*} \right)^{-1} v_b \left(\frac{\kappa_v \alpha_{PT}}{1 + \alpha_{PT}} \right)^2 \\ &\times \left(\frac{g_*}{100} \right)^{-\frac{1}{3}} \left(\frac{f}{f_{\text{peak}}^{\text{sw}}} \right)^3 \left[\frac{7}{4 + 3(f/f_{\text{peak}}^{\text{sw}})^2} \right]^{7/2} \end{aligned} \quad (\text{A1})$$

with the peak frequency [64–66]:

$$f_{\text{peak}}^{\text{sw}} = 1.9 \times 10^{-5} \frac{\beta}{H_*} \frac{1}{v_b} \frac{T_*}{100} \left(\frac{g_*}{100} \right)^{\frac{1}{6}} \text{Hz}. \quad (\text{A2})$$

Prior parameters [40]:

- α_{PT} , the latent heat;
- β/H_n , the inverse time duration of FOPT rescaled by H_n which is the Hubble parameter at the nucleation temperature, T_n ;
- T_* , the temperature when GWs are produced. Approximately, we have $T_* \approx T_n$;
- v_b , the velocity of vacuum bubble wall in the plasma background;

Other parameters [40, 67–71]:

- $\tau_{\text{sw}} = \min \left[\frac{1}{H_*}, \frac{R_*}{\bar{U}_f} \right]$, the duration of the sound-wave period. H_* is the Hubble parameter at T_* ;
- R_* , the mean bubble separation. The following equality holds, $H_* R_* = v_b (8\pi)^{1/3} (\beta/H_*)^{-1}$;
- $\bar{U}_f^2 \approx \frac{3}{4} \frac{\kappa_v \alpha}{1 + \alpha}$, the root-mean-square (RMS) fluid velocity. $\alpha = \alpha_{PT} (1 - \kappa_{\text{col}})$ where $\kappa_{\text{col}} \equiv E_{\text{wall}}/E_V$ is the proportion of the vacuum energy to accelerate the bubble wall [67];
- κ_v , the proportion of the vacuum energy transferred into the bulk fluid motion. It can be obtained via the hydrodynamic treatment of the plasma fluid [72].
- g_* , the effective number of degrees of freedom of relativistic species in the cosmic plasma at the time of GW formation.

b. Cosmic strings

GW spectrum [46, 73, 74]:

$$\Omega_{\text{GW}}^{\text{cs}}(f) = \sum_k \Omega_{\text{GW}}^{(k)}(f) \quad (\text{A3})$$

where for each k mode,

$$\begin{aligned} \Omega_{\text{GW}}^{(k)}(f) &= \frac{1}{\rho_c} \frac{2k}{f} \frac{\mathcal{F}_\alpha \Gamma^{(k)} G \mu^2}{\alpha_{CS} (\alpha_{CS} + \Gamma G \mu)} \int_{t_F}^{t_0} d\tilde{t} \frac{C_{\text{eff}}(t_i^{(k)})}{t_i^{(k)4}} \\ &\times \left[\frac{a(\tilde{t})}{a(t_0)} \right]^5 \left[\frac{a(t_i^{(k)})}{a(\tilde{t})} \right]^3 \Theta(t_i^{(k)} - t_F). \end{aligned} \quad (\text{A4})$$

Prior parameters:

- $G\mu$, where G is the gravitational constant and μ is the string tension;
- α_{CS} , the loop size parameter.

Other parameters:

- $\rho_c = 3H_0^2/8\pi G$, the critical density of the Universe;
- \mathcal{F}_α characterizes the proportion of the energy released by long strings, which we take as 0.1;
- C_{eff} characterizes the loop production efficiency, which we take as 5.4 and 0.39 for the radiation- and matter-dominated Universe respectively [46];
- $\Gamma \approx 50$ is the gravitational emission efficiency of loops [56];
- $\Gamma^{(k)} = \frac{\Gamma k^{-\frac{4}{3}}}{\sum_{m=1}^{\infty} m^{-\frac{4}{3}}}$ are the Fourier modes of cusps [55, 56, 75]; where $\sum_{m=1}^{\infty} m^{-\frac{4}{3}} \approx 3.60$ and $\sum_k \Gamma^{(k)} = \Gamma$.
- The formation time of loops of the k -mode:

$$t_i^{(k)}(\tilde{t}, f) = \frac{1}{\alpha_{CS} + \Gamma G \mu} \left[\frac{2k}{f} \frac{a(\tilde{t})}{a(t_0)} + \Gamma G \mu \tilde{t} \right]. \quad (\text{A5})$$

where \tilde{t} is the GW emission time;

- t_F , the formation temperature, after which cosmic string network reaches an attractor scaling regime;
- If cusps dominate the small-scale structure of loops, the high mode and the low mode are related as: $\Omega_{\text{GW}}^{(k)}(f) = \frac{\Gamma^{(k)}}{\Gamma^{(1)}} \Omega_{\text{GW}}^{(1)}(f/k) = k^{-4/3} \Omega_{\text{GW}}^{(1)}(f/k)$.

c. Domain walls

GW spectrum [11, 76, 77]:

$$\Omega_{\text{GW}}^{\text{dw}}(f)h^2 = \Omega_{\text{GW}}^{\text{peak}} h^2 S^{\text{dw}}(f) \quad (\text{A6})$$

where the peak GW amplitude is

$$\begin{aligned} \Omega_{\text{GW}}^{\text{peak}} h^2 &\approx 5.20 \times 10^{-20} \times \tilde{\epsilon}_{\text{gw}} \mathcal{A}^4 \left(\frac{10.75}{g_*} \right)^{1/3} \\ &\times \left(\frac{\sigma}{1 \text{TeV}^3} \right)^4 \left(\frac{1 \text{MeV}^4}{\Delta V} \right)^2, \end{aligned} \quad (\text{A7})$$

and the shape function is

$$S^{\text{dw}}(f) = (f/f_{\text{peak}}^{\text{dw}})^3, \quad f < f_{\text{peak}}^{\text{dw}} \quad (\text{A8})$$

$$S^{\text{dw}}(f) = (f/f_{\text{peak}}^{\text{dw}})^{-1}, \quad f \geq f_{\text{peak}}^{\text{dw}} \quad (\text{A9})$$

with the peak frequency [11]

$$f_{\text{peak}}^{\text{dw}} \simeq 3.99 \times 10^{-9} \text{Hz} \mathcal{A}^{-\frac{1}{2}} \left(\frac{1 \text{TeV}^3}{\sigma} \right)^{\frac{1}{2}} \left(\frac{\Delta V}{1 \text{MeV}^4} \right)^{\frac{1}{2}}. \quad (\text{A10})$$

Prior parameters:

- σ , the domain wall tension;
- ΔV , the bias potential that explicitly breaks the degeneracy of vacua which makes the domain wall to disappear and thus marks the location of peak frequency.

Other parameters:

- $\mathcal{A} = 1.2$, the area parameter whose value can be obtained via numerical simulations [11, 76];
- $\tilde{\epsilon}_{\text{gw}} = 0.7$, the efficiency parameter of generating GWs [11].

d. Scalar-induced GWs

GW spectrum [51]:

$$\begin{aligned} \Omega_{\text{GW}}^{\text{si}}(f)h^2 &= \frac{1}{12} \Omega_{\text{rad}} h^2 \left(\frac{g_0}{g_*} \right)^{\frac{1}{3}} \\ &\times \int_0^\infty dv \int_{|1-v|}^{1+v} du \left(\frac{4v^2 - (1+v^2-u^2)^2}{4uv} \right)^2 \\ &\times P_{\mathcal{R}}(2\pi fu) P_{\mathcal{R}}(2\pi fv) I^2(u, v), \end{aligned} \quad (\text{A11})$$

where

$$\begin{aligned} I^2(u, v) &= \frac{1}{2} \left(\frac{3}{4u^3 v^3 x} \right)^2 (u^2 + v^2 - 3)^2 \\ &\times \left\{ \left[-4uv + (u^2 + v^2 - 3) \ln \left| \frac{3 - (u+v)^2}{3 - (u-v)^2} \right| \right]^2 \right. \\ &\left. + \left[\pi (u^2 + v^2 - 3) \Theta(u+v - \sqrt{3}) \right]^2 \right\}. \end{aligned} \quad (\text{A12})$$

$P_{\mathcal{R}}(k)$ is the power spectrum of curvature perturbations. We consider the case that $P_{\mathcal{R}}(k)$ has a power-law form around $k_* = 2\pi f_* = 20.6 \text{ pc}^{-1}$ (where $f_* = 1 \text{ yr}^{-1}$),

$$P_{\mathcal{R}}(k) = P_{\mathcal{R}0} \left(\frac{k}{k_*} \right)^m \Theta(k - k_{\text{min}}) \Theta(k_{\text{max}} - k), \quad (\text{A13})$$

$\Theta(x)$ is the Heaviside function. Note: to prevent overproduction of PBHs, we set cutoffs at $k_{\text{min}} = 0.03 k_*$ and $k_{\text{max}} = 100 k_*$ so that there is an upper bound on $P_{\mathcal{R}}(k)$.

Prior parameters:

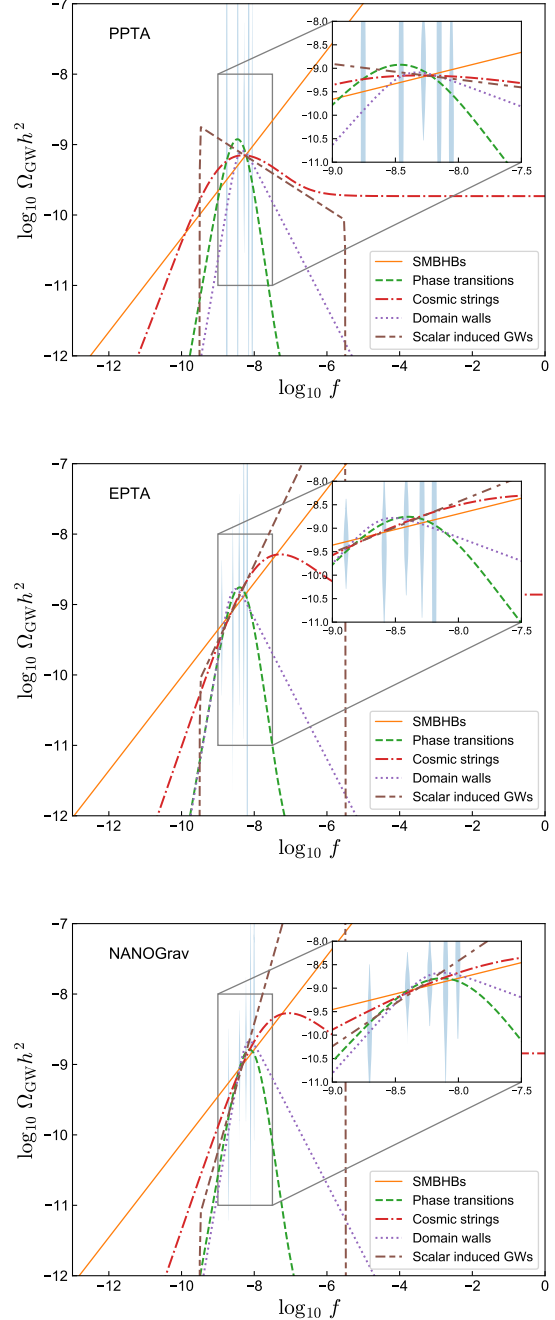


Figure 6. The GW energy spectra derived from different models employing the best-fit parameters from current new datasets of PPTA, EPTA and NANOGrav. The violin plots represent the first five frequency bins of the corresponding datasets.

- $P_{\mathcal{R}0}$, the power spectrum of scalar perturbations at $k = k_*$;
- m , the slope of the power spectrum of scalar perturbations.

Other parameters:

- g_0 , the present-day effective number of degrees of freedom of relativistic species;
- $\Omega_{\text{rad}}h^2 = 4.2 \times 10^{-5}$, the present-day abundance of radiation.

e. Plots of GW spectra

The GW spectra from different sources confronting with the low-frequency five bins data of NANOGrav 15-yr, EPTA release-2 and PPTA DR3 are shown in Fig. 6.

Appendix B: Bayesian method

Following Ref. [26], we briefly summarize here the Bayesian method for model comparisons and model fitting.

Basically, Bayes' theorem gives

$$P(M|D) = P(D|M) \frac{P(M)}{P(D)} \quad (\text{B1})$$

where D and M respectively represent data and model. We also have

$$P(D|M) = \int P(D|\theta, M)P(\theta|M)d\theta. \quad (\text{B2})$$

To compare two models, M_i and M_j , we calculate the ratio

$$O_{ij} \equiv \frac{P(M_i|D)}{P(M_j|D)} = \frac{P(D|M_i) P(M_i)}{P(D|M_j) P(M_j)} = B_{ij} \frac{P(M_i)}{P(M_j)}. \quad (\text{B3})$$

The ratio between the prior odds, $P(M_i)/P(M_j)$, is usually assumed to be close to 1. $B_{ij} \equiv P(D|M_i)/P(D|M_j)$ is the Bayes factor for M_i vs. M_j .

The task of model fitting is to find the posterior distributions $P(\theta|D, M)$ of parameters θ for known data D and model M . Again, Bayes' theorem gives

$$P(\theta|D, M) = \frac{P(D|\theta, M)P(\theta|M)}{P(D|M)}, \quad (\text{B4})$$

The conditional probabilities $P(D|\theta, M)$, $P(\theta|M)$, and $P(D|M)$ are, respectively, the likelihood, prior, and, model evidence.

As discussed in the main text, we have presented the model comparisons in eqs. (1)-(3) based on Bayes factors. We have utilized the datasets of NANOGrav 15-yr dataset, EPTA release-2, and PPTA DR3 and the SGWB models of SMBHB, FOPT, cosmic strings, domain walls, and large amplitude curvature perturbations. The results of model fitting have also been shown in Figs. 1-5, with the help of `emcee` and `GetDist` [78, 79].

Table II. Model parameters and their prior distribution in data analysis. U and log-U stand for the uniform and log-uniform distribution.

Parameter	Description	Prior
SMBHB		
A	amplitude	log-U[-18, -12]
FOPT		
β/H_*	inverse PT duration	U[5, 70]
T_*	PT temperature	U[0.01, 1.6]
α_{PT}	PT strength	U[0.0, 1.0]
v_b	velocity of bubble wall	U[0.9, 1.0]
Cosmic string		
$G\mu$	string tension	log-U[-12, -6]
α_{CS}	loop-size parameter	log-U[-6, 0]
Domain wall		
σ	surface energy density	log-U[0, 8]
ΔV	bias potential	log-U[0, 8]
Curvature perturbations		
$P_{\mathcal{R}0}$	amplitude of spectrum	log-U[-4, -1.5]
m	slope of spectrum	U[-2, 2]